Materials Research Bulletin 47 (2012) 744–749

Contents lists available at SciVerse ScienceDirect

Materials Research Bulletin

journal homepage: www.elsevier.com/locate/matresbu

Growth, structural and optical characterizations of $LiLa_{(1-x)}Eu_x(WO_4)_2$ single-crystalline fibers by the micro-pulling-down method

Jair Ricardo de Moraes [a], Sonia Licia Baldochi [a,*], Leonardo dos Reis Leano Soares [a], Vera Lucia Mazzocchi [a], Carlos Benedicto Ramos Parente [a], Lilia Coronato Courrol [b]

[a] Instituto de Pesquisas Energéticas e Nucleares, IPEN – CNEN/SP, 05508-000 São Paulo, SP, Brazil
[b] Departamento de Ciências Exatas e da Terra, Universidade Federal de São Paulo, UNIFESP, 09972-270 Diadema, SP, Brazil

ARTICLE INFO

Article history:
Received 8 September 2011
Received in revised form 21 November 2011
Accepted 8 December 2011
Available online 17 December 2011

Keyword:
A. Oxides
B. Crystal growth
D. Crystal structure
D. Luminescence
D. Optical properties

ABSTRACT

Transparent and uniform $LiLa_{(1-x)}Eu_x(WO_4)_2$ single-crystalline fibers where $x = 0.005$, 0.01, 0.03, 0.05, 0.07, 0.1, 0.15, 0.2, 0.25 and 1.0, with an average of 20–40 mm length were obtained by the micro-pulling-down method aiming structural and optical characterization. The optimum pulling rate was found to depend on the difference between alkali and rare earth ionic radii. Rietveld analysis from X-ray diffraction data and excitation spectroscopy at room temperature were applied to investigate the lattice changes due to the Eu^{3+} incorporation in the host. $LiLa_{(1-x)}Eu_x(WO_4)_2$ crystal fibers present red emission due to the electric dipole $^5D_0 \rightarrow {}^7F_2$ transition under 395 nm excitation showing a concentration quenching around 20 mol% of doping. The excitation spectra of the $^7F_0 \rightarrow {}^5D_0$ transition show small changes in the Eu^{3+} surroundings as function of dopant concentration.

1. Introduction

In the last years, rare earth activated $LiLa(WO_4)_2$ (LLW) single crystals have gained much attention because of their suitable optical properties to design luminescent materials. In fact, spectroscopic characteristics were reported for Nd^{3+} and Yb^{3+}-doped [1–4] and Er^{3+}/Yb^{3+} co-doped [5] bulk crystals. The thermal and mechanical properties of LLW, comparable to other tungstates, make it a promising host for solid state laser devices [2]. This crystal belongs to the $M(RE)(XO_4)_2$ family where M = monovalent alkali metals, RE = trivalent rare earth elements and X = Mo^{6+} and W^{6+}. It possesses relatively low melting point (1065 °C) and no phase transitions upon cooling (under atmospheric pressure) [6], allowing the single crystal growth directly from the melt. It crystallizes in the tetragonal scheelite ($CaWO_4$) structure type with space symmetry group $I4_1/a$ and shows partial disorder, i.e., Li^+ and La^{3+} ions share the same crystallographic positions [6–8]. The partial disorder could lead, in some cases, to the splitting of the optical lines resulting of a multisite structure (different configurations in the first cationic coordination sphere). Consequently, the inhomogeneously broadened absorption and luminescence bands observed in similar tungstates [9,10] may be considered as an advantage mainly for laser applications since for laser emission wider absorption lines result in an efficient pumping, while wider emission lines means tuneability.

At the same time, the interest on Eu-based or Eu-doped double molybdates and tungstates have arisen because of their strong red luminescence and chemical stability under UV light excitation and appropriate chromaticity that makes them promising candidates for developing new red phosphor components for white light emitting diodes (W-LED) [11–13].

The growth of single crystal fibers has been established as a low cost and fast process for obtaining samples comparatively to the bulk growth for several studies on thermal, compositional and optical properties [14,15]. Concerning the geometry of these crystals, the as-grown fiber shape is near-ready for applications and it is suitable to nonlinear optical interactions, whose efficiencies can be greatly enhanced by the long interaction lengths and tight beam confinement available in guided wave structures. Its reduced dimension is also an attractive for developing compact devices.

In our understanding, very few works were reported about single crystal fibers growth of double tungstates. Recently, it has been studied as single crystal fibers: Nd-doped $NaGd(WO_4)_2$ (NGW) [16], $NaLa(WO_4)_2$ (NLW) [17] and LLW [18] to characterize their optical properties. Additionally, we also investigated the growth process of pure and Yb^{3+} and Nd^{3+}-doped LLW single crystals fibers by the micro-pulling-down method (μ-PD) [19] regarding the meniscus behavior, effect of pulling rate changes and liquid evaporation. In this work we report for the first time the

* Corresponding author. Tel.: +55 11 3133 9355; fax: +55 11 3133 9374.
E-mail addresses: baldochi@ipen.br, jairric@yahoo.com.br (S.L. Baldochi).

0025-5408/$ – see front matter © 2011 Elsevier Ltd. All rights reserved.
doi:10.1016/j.materresbull.2011.12.007

growth by the μ-PD of $LiLa_{(1-x)}Eu_x(WO_4)_2$ single crystal fibers where $x = 0.005–1.0$. Structural and optical characterizations were carried out for verifying the effects of disorder in the doped host. Site-selective excitation spectroscopy at room temperature (RT) was employed to investigate substitution sites for Eu^{3+}.

2. Experimental setup

The starting material for fiber growth was synthesized through a solid state reaction method from analytical grade chemicals – Li_2CO_3, La_2O_3 and Eu_2O_3 (99.98%), and WO_3 (99.998%) – in the appropriate amount in accordance with the following reactions:

$$(1/2)Li_2CO_3 + (1/2)La_2O_3 + 2WO_3 \rightarrow LiLa(WO_4)_2 + CO_2\uparrow \quad (1)$$

$$(1/2)Li_2CO_3 + (1/2)Eu_2O_3 + 2WO_3 \rightarrow LiEu(WO_4)_2 + CO_2\uparrow \quad (2)$$

$$(1-x)LiLa(WO_4)_2 + xLiEu(WO_4)_2 \rightarrow LiLa_{(1-x)}Eu_x(WO_4)_2 \quad (3)$$

with $x = 0.005$, 0.01, 0.03, 0.05, 0.07, 0.1, 0.15, 0.2, 0.25 and 1.0 (nominal concentrations). The reagents powder mixtures were annealed in a single step under air atmosphere. The treatment of the material was performed in platinum crucibles. The powders were heated at a rate of 50 °C/h to 750 °C/h and treated in this temperature for a period of 48 h and then cooled down to RT. The formation of both tungstates was confirmed through X-ray powder diffraction (XRD) analysis. The doping composition of each particular starting charge for crystal growth was obtained by mixing appropriated fractions of each tungstate in accordance with Eq. (3).

Single-crystalline fibers were grown in a modified commercial resistive μ-PD apparatus [19], in Pt–Au (5%) home-made crucibles with an inner capillary diameter of 0.8 mm and 1.2 mm length. An addition of 5 mol% $Li_2W_4O_{13}$ to the melt was found to increase the quality of the fibers considerably. The crystal fiber pulling was done with rates ranging from 0.06 to 0.18 mm/min under air atmosphere. A LLW crystal fiber was used as seed. Ended the growth, the crystal fibers were cooled down to RT in 30 min. The visual control of the fiber growth was performed with a stereo microscope and a CCD camera.

The fibers were analyzed through a video-microscope to evaluate macroscopic defects (cracks, bubbles and inclusions) and segregation. The crystallization of the Eu:LLW and $LiEu(WO_4)_2$ (LEW) was confirmed through XRD analysis in a Rigaku DMAXB diffractometer, equipped with a curved graphite monochromator and Co cathode ($\lambda_{K\alpha} = 1.7889$ Å). The data for analyses were obtained at RT in the range of 2θ from 15° to 120° with a step scan rate of 0.013°/5 s. All measurements were performed on powders. Our experimental data and XRD patterns published by Postema et al. [20] for LLW and LEW and, by Chiu et al. [13] for LEW were compared. Rietveld refinement was carried out by the GSAS software [21].

Samples of Eu:LLW and LEW crystal fibers with dimensions ~0.8 mm diameter and 10.0 mm length were used for spectroscopic characterization. The fluorescence spectrum and fluorescence lifetime were measured using a Horiba Fluorolog 3 modular fluorimeter at RT. The fiber was excited perpendicular to its length.

3. Results and discussion

3.1. Fiber crystal growth

Single crystal fibers of Eu:LLW and LEW with diameter of ~0.7–0.8 mm and from 20 to 40 mm length were successfully obtained (Fig. 1). They were transparent with colors varying from colorless to yellow depending on the Eu concentration, except for the LEW fibers that were slightly pink in color. Only the LEW single crystal fibers presented cracks, probably due to thermal stress under cooling. The fibers were uniform in diameter (nearly circular) and without any evidence of macroscopic segregation (Fig. 1b and d).

In the previous work it was verified that liquid overheating leads to the increasing of the meniscus height compromising the growth stability [19]. However, this can be compensated by an accurate control of the growth system power and, fibers can be grown homogenous in diameter under a stable liquid zone (meniscus) and flat liquid–solid interface. The optimal average meniscus height was about 150 μm and no bubbles were observed in the meniscus or in the fibers. No significant evaporation was observed upward the growth camera during or at the end of the experiments.

It was observed for all compositions starting from 3 mol% of Eu-doping that a larger pulling rate could be used without compromising their surface and optical quality, compared to undoped LLW: the rate could be increased from 0.06 mm/min (pure LLW) to a maximum of 0.18 mm/min (≥3 mol% Eu doping). This observation can be discussed based on an approach by Maier et al. [8] for the study of polymorphism in double molybdates and tungstates belonging to the $M(RE)(XO_4)_2$ group. Let

$$\Delta r = |r_{ion}(M^+) - r_{ion}(RE^{3+})| \quad (4)$$

and

$$r_{av} = \frac{r_{ion}(M^+) + r_{ion}(RE^{3+})}{2} \quad (5)$$

be the radius difference, and the average radius, respectively of both M^+ (Li^+, Na^+) and RE^{3+} (La^{3+}, Eu^{3+}). M^+ as well as RE^{3+} are substituting for Ca^{2+} in the original scheelite structure of $CaWO_4$. It turns out that a large radius difference Δr as well as a large deviation of r_{av} from the calcium size $r_{ion}(Ca^{2+}) = 1.12$ Å results in

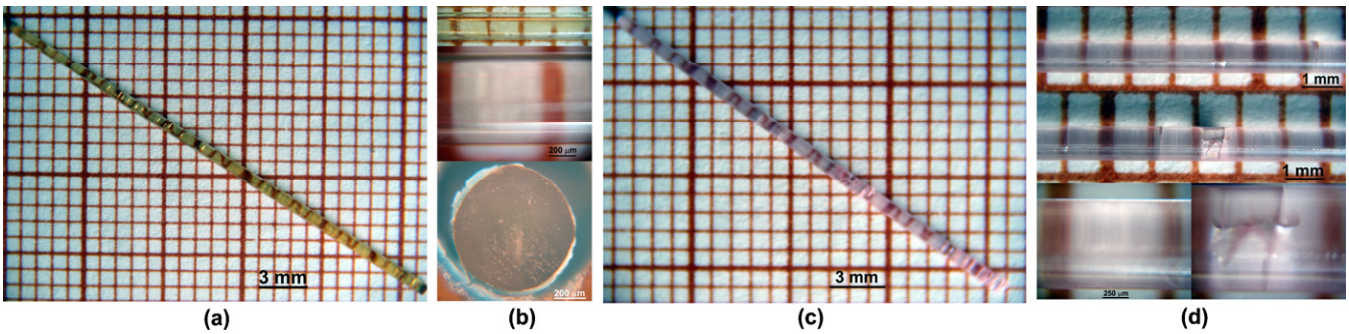

Fig. 1. As-grown single-crystalline fibers obtained through the μ-PD method in the resistive mode of (a) 10 mol% Eu-doped LLW, (b) the details show fiber surface without irregularities and the near-circular diameter section (slightly polished), (c) LEW, (d) the details show regions of the LEW fiber without cracks, even after few hours of growth and with cracks probably due to thermal stress under cooling. The fiber surface presents no irregularities.

Table 1
Comparison between applied pulling rates for LLW fiber growth and ionic radii of the constituents.

Crystals	Δr (Å)	r_{av} (Å)	$r_{ion}(M^+)/r_{ion}(RE^{3+})$	μ-PD pulling rate (mm/min)	Ref.
LLW; Nd:LLW	0.24	1.04	0.79	0.06	[18,19]
Eu:LLW (from 3 mol%) and LEW	0.14	0.99	0.87	0.18	This work
Nd:NLW	0.02	1.17	1.02	0.36	[17]

The ionic radii considered are the ones reported by Shannon [23]: Li (0.92 Å), Na (1.18 Å), La (1.16 Å), Eu (1.06 Å) and Ca (1.12 Å).

larger crystal structure distortion, and finally in an ordered distribution of the alkaline and rare earth ions. Only if the size ratio between both ions is sufficiently small, the distribution remains statistically disordered. Kolesov and Kozeeva [22] reported that the limit value $r_{ion}(M^+)/r_{ion}(RE^{3+}) = 1.30–1.32$ separates ordered from disordered distribution. A smaller ratio results in a disordered distribution, and subsequently in a strained structure. Table 1 reports the influence of ionic sizes on appropriate growth rates for some cases from the literature and from this study.

According to the growth kinetics theory in atomic scale [24,25], a crystal grows by the addition of atoms from the melt in the crystal correspondent positions in the growth interface that depends only of the local conditions like temperature, composition and capillary effect. Considering that the net crystallization rate is atoms size dependent, the hypothesis that the pulling rate decreases as higher is the ionic radii difference between the alkali and rare earth constituents is consistent with the data presented in Table 1.

In the case of NLW ($NaLa(WO_4)_2$), Na and La possess very similar ionic radii and a competition between both should be not expected for their adding in the crystal interface. However, for Li and La on the LLW case, the difference is so significant that leads to a situation of competition which makes it necessary to decrease the pulling rate in order to allow the addition of these atoms in the most probable sites of the growth interface. Regarding that the atomic mobility in the interface is cooperative and the ordering of one region affects other interface regions, the addition of Eu in the LLW would stabilize this competition contributing for the ionic radii difference reduction among the occupants of the same crystallographic position, i.e., Li, La and Eu.

3.2. Structural characterization of the fiber crystals

The XRD patterns reveal the crystallization of the tetragonal scheelite-like fibers occurs as a unique phase for all compositions, from LLW to LEW (Fig. 2). It is important to comment that the structure of LEW crystals is still not well defined and, in fact, it is very ambiguous in the literature. In the 1970s, Klevtsov [26] described the LEW structure as being isomorphous to the scheelite-like tetragonal system presenting a scheelite modification that is not specified, in samples obtained by spontaneous crystallization from fused solution. Trunov [7] and later Klevtsov [27] describes a polymorphic transition from the tetragonal ($I4_1/a$) to the monoclinic system ($P2/c$) from samples prepared via solid state reaction. Recently, Chiu [13] reported the LEW crystalline structure as belonging to the triclinic system ($P1^-$) with samples obtained via solid state reaction. However, Hwang [28] obtained nanoparticles of LEW via the sol–gel method and Postema [20] powders via the solid state reaction, both authors describing its structure as a scheelite-like tetragonal system ($I4_1/a$).

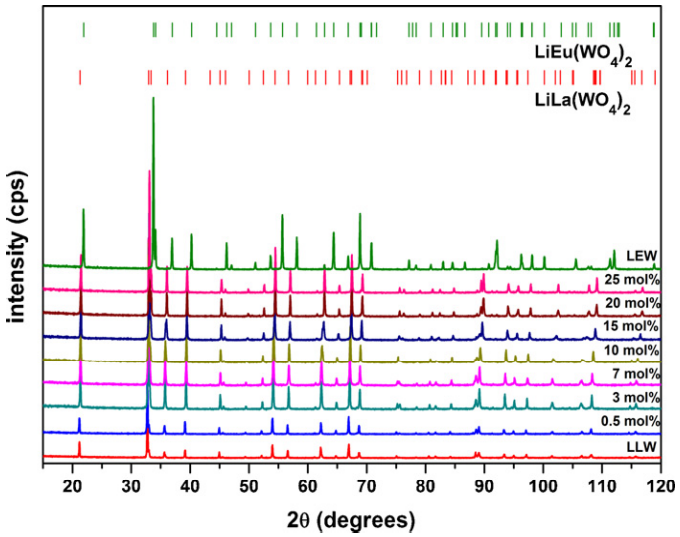

Fig. 2. XRD patterns of $LiLa_{(1-x)}Eu_x(WO_4)_2$ single crystal fibers in the compositions of 0, 0.5, 3, 7, 10, 15, 20, 25 and 100 mol%.

Comparing triclinic, monoclinic and tetragonal diffraction patterns with our starting material for fiber growth (prepared via solid state reaction) and single crystal fiber powder diffraction data it is clear to notice that both triclinic and monoclinic should present extra diffraction peaks that do not appear in our experimental data. During the Rietveld analysis for all compositions (LLW, Eu:LLW and LEW), the following possibilities were considered: only a tetragonal phase, tetragonal plus triclinic or monoclinic phases together and the triclinic or monoclinic phases alone. The best results were achieved with only the tetragonal phase as showed as example in Fig. 3a (LLW) and 3b (LEW). The analysis of the emission spectroscopy data (Section 3.3) corroborates our conclusion about the tetragonal structure.

The observed reductions for the lattice parameters and volume (Fig. 4 and Table 2) are reasonable with the Eu incorporation. Such reductions are expected since the Eu atoms are smaller and more electronegative than the La atoms. For that reason, a lattice contraction should occur with oxygen atoms becoming closer to the cations in the structure.

Considering that the length reductions for Li/La/Eu–O and W–O bonds may occur, in the region of 2θ between 87° and 93°, the peaks indexed by {1 4 1} and {2 0 8} start to be separated at 10 and 15 mol% of Eu (Fig. 5). At 20 and 25 mol% they appear completely apart. One can assume that this splitting is due to the distortion induced by the Eu incorporation.

3.3. Optical characterization of the fiber crystals

Fig. 6 shows the excitation and emission spectra of the 0.5 mol% doped Eu^{3+}:LLW fiber crystal. The excitation spectrum monitored at 616 nm, corresponding to the $^5D_0 \rightarrow {}^7F_2$ emission of Eu^{3+} ion, consists of some sharp lines. In the range of 350–550 nm the sample shows characteristic intra-configurational $4f^n$–$4f^n$ transitions of Eu^{3+}; sharp $^7F_0 \rightarrow {}^5L_6$ transition for 393 nm, $^7F_0 \rightarrow {}^5D_2$ transition for 464 nm and the $^7F_0 \rightarrow {}^5D_1$ transition for 535 nm. In the fluorescence spectrum obtained exciting the single fiber sample at 393 nm, shown in this same figure, with wavelength ranging from 580 to 720 nm, five group transitions were recognized: $^5D_0 \rightarrow {}^7F_0$, $^5D_0 \rightarrow {}^7F_1$, $^5D_0 \rightarrow {}^7F_2$, $^5D_0 \rightarrow {}^7F_3$ and $^5D_0 \rightarrow {}^7F_4$. The line assignments were made by analogy to the Eu^{3+} transitions observed in other tungstate hosts [29–31].

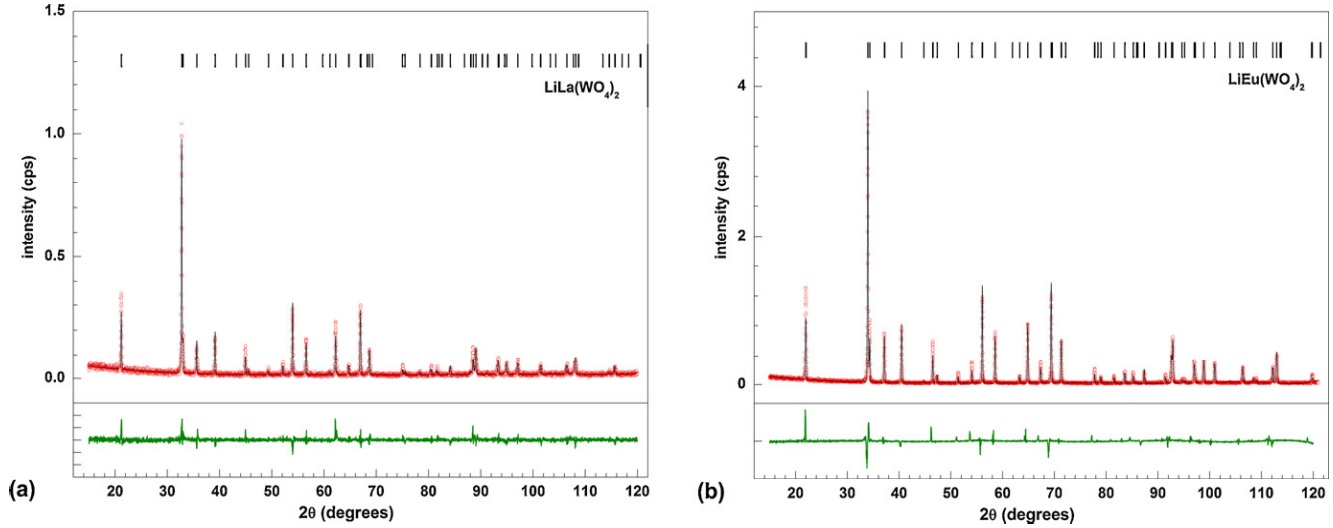

Fig. 3. Rietveld refinement of XRD data of (a) LLW and (b) LEW single crystal fibers.

The allowed electric-dipole transition would be dominant when Eu^{3+} occupies the lattice site of noncentrosymmetric environment in the scheelite phases [29,30]. The $^5D_0 \rightarrow {}^7F_2$ transition intensity is much larger than that of the $^5D_0 \rightarrow {}^7F_1$. The dominance of the forced electric-dipole transition indicates that Eu^{3+} ions occupy no inversion center sites in the Eu:LLW single crystal fibers similar to observed in other double tungstate hosts [29–32].

The increasing of Eu concentration up to ~20 mol% of doping in the LLW host enhances its luminescence intensities (Fig. 7). Concentration quenching and a slightly shift towards longer wavelengths were observed for higher values of doping. The intensities of Eu:LLW doped with low concentrations (1 and 3 mol%) and LEW are comparable. The weak LEW luminescence is clearly related to distortions in the structure of the crystal around the Eu site environment even keeping the eightfold coordination.

Trivalent europium (Eu^{3+}) is known as a spectroscopic probe because it possesses a simple $^{2S+1}L_J$ structure with non-degenerated $^7F_0$ ground and $^7D_0$ first excited states. The most probable $^5D_0 \rightarrow {}^7F_2$ transition is due to the electric dipole transition that is very sensitive to relatively small changes in the surroundings, over the less probable $^5D_0 \rightarrow {}^7F_1$ magnetic dipole transition that is insensitive to the environment [32]. Hence, the ratio R between $^5D_0 \rightarrow {}^7F_2$ and $^5D_0 \rightarrow {}^7F_1$ integral intensities is a good measure for the symmetry of the Eu^{3+} site in the crystal host which indicates the relative magnitude of the local hypersensitivity. High ratios suggest an enhancement of the electric dipole transition and the strengthening of the crystal field. Fiber crystals with low doping (0.5–10 mol%) presented $R \sim 9$ while for higher concentrations, including LEW, $R \sim 10$ indicating a slightly distortion in the coordination of the europium active site when its concentration increases in the LLW host.

Because the splitting of the $^5D_0$ energy level of the Eu^{3+} ions is affected by crystal field, its fluorescence spectra for $^5D_0 \rightarrow {}^7F_J$ transition have $2J + 1$ lines; so the site symmetry of Eu^{3+} in LLW can be studied considering the number of stark splitting. It is possible to map the $^5D_0 \rightarrow {}^7F_0$ emission, exciting samples around 526 nm (Fig. 8). These spectra should contain only one band. However, it is possible to verify that there are 2 bands at 577 and 580 nm. Low concentrations at lower wavelengths show lower intensities than those at higher wavelengths. This proportion rises as Eu concentration increases up to ~20 mol%. The band at 580 nm can be explained by the characteristic emission of Eu^{3+} since the undoped LLW does not present it. In other hand, the band at 577 nm probably is due to the $(WO_4)^{2-}$ group because of its presence for all samples compared. In fact, tungstate group present

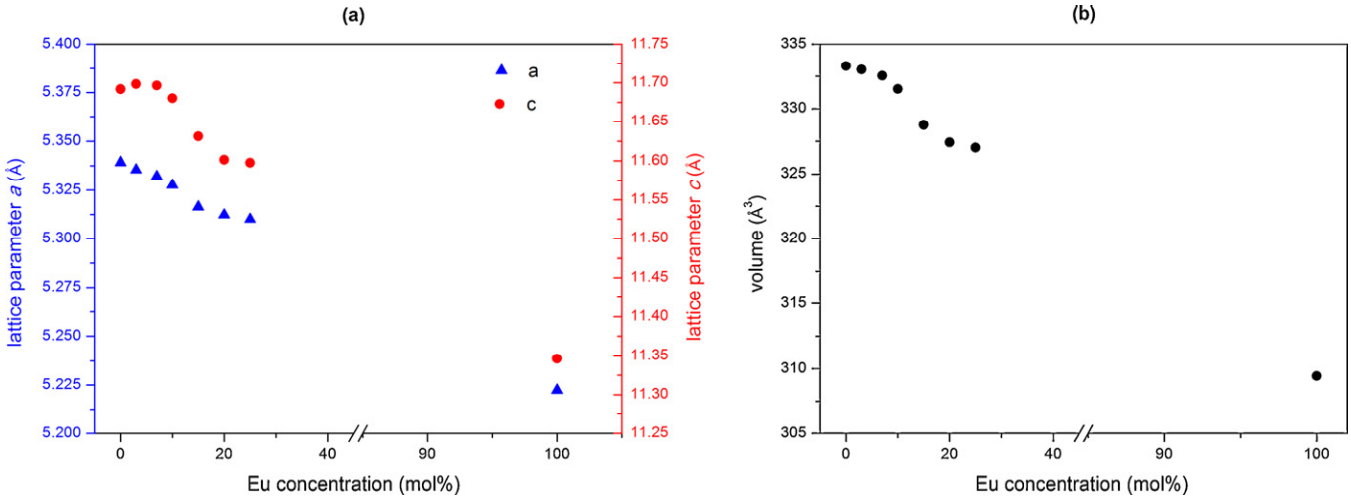

Fig. 4. (a) Lattice parameters and (b) volume of $LiLa_{(1-x)}Eu_x(WO_4)_2$ crystal fibers as function of Eu concentration.

Table 2
Refined crystallographic data of $LiLa_{(1-x)}Eu_x(WO_4)_2$ at room temperature.

Fiber crystal	LLW	0.5 mol%	3 mol%	7 mol%	10 mol%	15 mol%	20 mol%	25 mol%	LEW
a (Å)	5.3392 (1)	5.3409 (1)	5.3355 (1)	5.3322 (1)	5.3276 (1)	5.3164 (1)	5.3123 (1)	5.3101 (1)	5.2224 (1)
c (Å)	11.6918 (2)	11.6855 (2)	11.6985 (2)	11.6967 (2)	11.6802 (2)	11.6313 (2)	11.6014 (2)	11.5976 (1)	11.3464 (1)
V (Å^3)	333.30 (1)	333.33 (1)	333.03 (1)	332.56 (1)	331.52 (1)	328.74 (1)	327.40 (1)	327.02 (1)	309.45 (1)
[a]Li/Ln (4a)	(0, 1/4, 1/8)	(0, 1/4, 1/8)	(0, 1/4, 1/8)	(0, 1/4, 1/8)	(0, 1/4, 1/8)	(0, 1/4, 1/8)	(0, 1/4, 1/8)	(0, 1/4, 1/8)	(0, 1/4, 1/8)
W (4b)	(1/2, 3/4, 1/8)	(1/2, 3/4, 1/8)	(1/2, 3/4, 1/8)	(1/2, 3/4, 1/8)	(1/2, 3/4, 1/8)	(1/2, 3/4, 1/8)	(1/2, 3/4, 1/8)	(1/2, 3/4, 1/8)	(1/2, 3/4, 1/8)
O (16f)									
x	0.7390 (19)	0.7601 (17)	0.7746 (12)	0.7707 (11)	0.7636 (14)	0.7524 (13)	0.7740 (13)	0.7733 (12)	0.7506 (15)
y	0.5951 (23)	0.5925 (21)	0.5840 (15)	0.5777 (15)	0.5939 (18)	0.5912 (16)	0.5885 (16)	0.5759 (17)	0.5924 (16)
z	0.0473 (9)	0.0461 (8)	0.0551 (6)	0.0533 (6)	0.0467 (7)	0.0447 (7)	0.0470 (6)	0.0457 (6)	0.0491 (7)
R_p	15.47	14.64	11.23	10.38	12.58	11.54	11.90	11.97	16.02
R_{wp}	20.16	18.76	14.54	13.29	16.67	15.21	15.30	15.23	21.25
χ^2	1.1	1.1	1.6	1.4	1.7	1.6	1.5	1.4	2.8

[a] Li and La are randomly distributed in the same site (occupation factor 0.5).

broad band emission in the region of 320–650 nm [30]. The lack of additional bands in the LEW $^5D_0 \rightarrow {}^7F_0$ emission corroborates the hypothesis of tetragonal structure for this crystal.

The crystalline structure of $LiLa(WO_4)_2$ has been identified to be isostructural to $CaWO_4$ (scheelite) with space group $I4_1/a$ (C_{4h}) [6,7,20]. The structure is built-up with WO_4 tetrahedral groups and LiO_8 and LaO_8 distorted square antiprisms. The Li^+ and La^{3+} ions occupy statistically a single position, with S_4 (C_2) site symmetry (a single lattice site 4*a* is 50% filled with Li^+ and 50% with the trivalent cations La^{3+} in a random distribution for the first cationic sphere of neighbors). Therefore, we conclude that the symmetry S_4 of the point site is slightly reduced when it is occupied by Eu^{3+} (which partially or totally replaces La^{3+} in the $LiLa_{(1-x)}Eu_x(WO_4)_2$ fiber crystals).

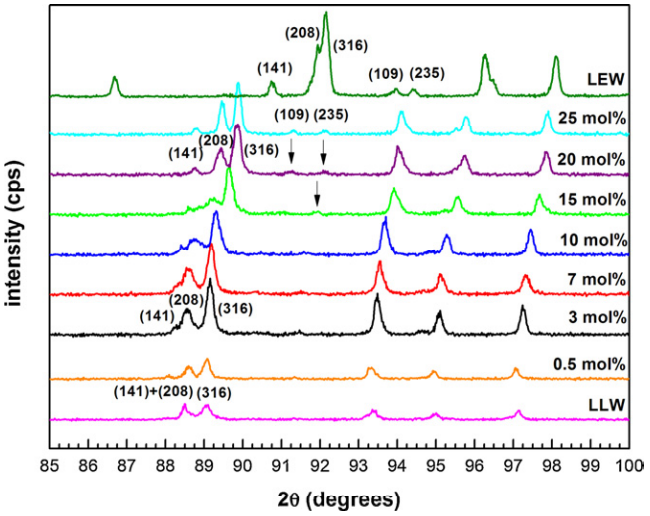

Fig. 5. XRD patterns on the 85–100° range showing the separation of the {1 4 1} and {2 0 8} group planes from 10 mol% and the appearing of the {1 0 9} and {2 3 5} group plans from 15 mol% of Eu.

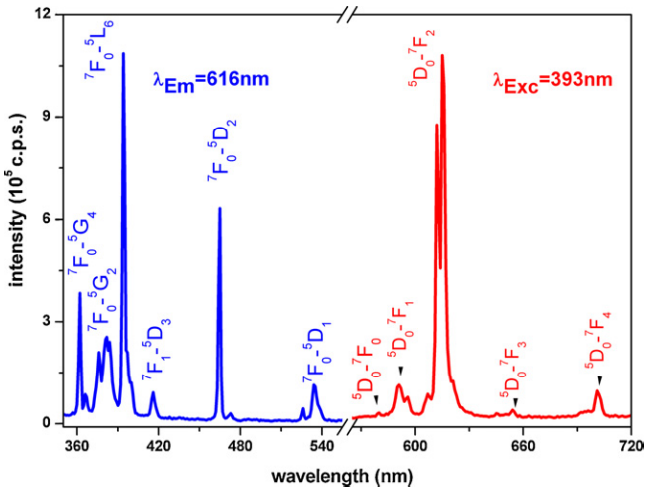

Fig. 6. Spectra of excitation (393 nm) and emission (616 nm) of a 0.5 mol% doped Eu^{3+}:LLW crystal fiber grown by the μ-PD growth.

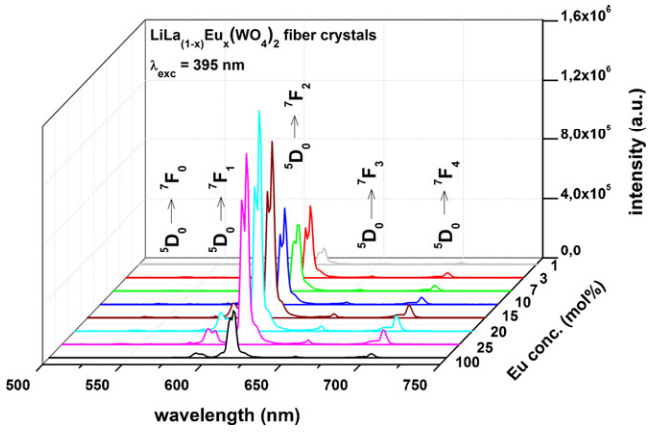

Fig. 7. (a) Emission spectra at RT of $LiLa_{(1-x)}Eu_x(WO_4)_2$ (x = 0.005, 0.03, 0.07, 0.10, 0.15, 0.20, 0.25, 1.0) crystal fibers under excitation at 395 nm. A concentration quenching is observed from 20 mol% of doping.

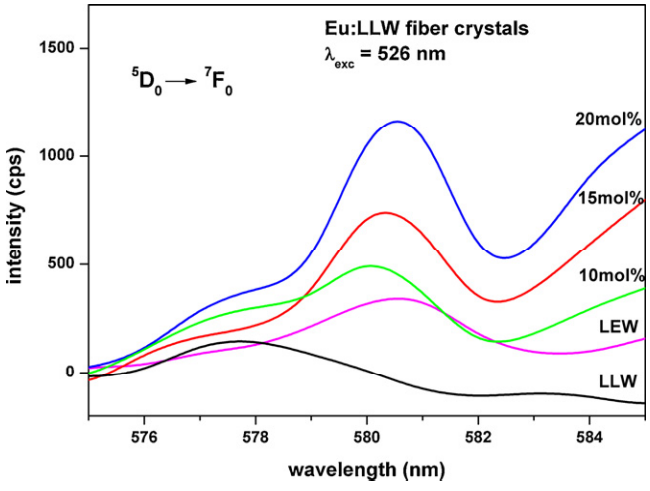

Fig. 8. Emission spectra of the $^5D_0 \rightarrow {}^7F_0$ transition obtained under 526 nm excitation of Eu:LLW fiber crystals (10, 15 and 20 mol%) compared to LLW and LEW fibers.

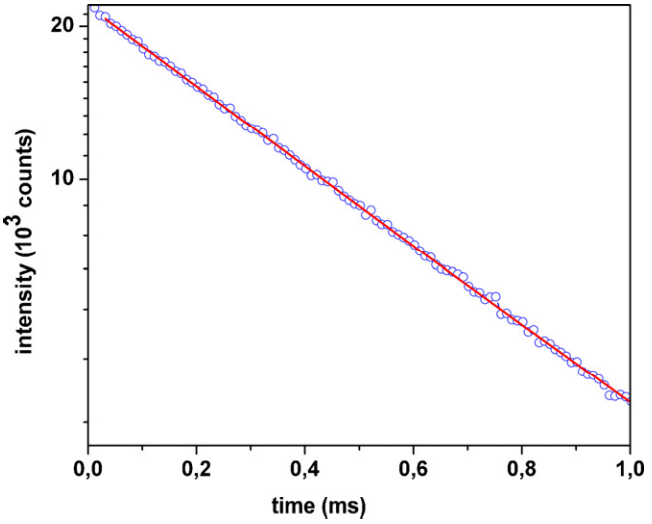

Fig. 9. $^5D_0$ level emission lifetime of 0.5 mol% doped Eu^{3+}:LLW crystal fiber obtained under excitation at 393 nm and emission at 616 nm.

Table 3
$^5D_0 \rightarrow {}^7F_2$ emission lifetime at RT of Eu^{3+} ions in different tungstates hosts.

Eu^{3+}-doped tungstates crystals	$^5D_0 \rightarrow {}^7F_2$ emission lifetime (μs)	References
$LiLa(WO_4)_2$ – fiber: 0.5 mol%	544	This work
$PbWO_4$ – bulk: 0.05 wt%	330	[33]
$PbWO_4$ – bulk: 0.01 at%	520	[34]
$NaLa(WO_4)_2$ – powder: 5.0 mol%	510–620	[35]

The luminescence decay curve of the $^5D_0$ level, obtained fixing the emission at wavelength 616 nm and exciting the sample at 393 nm, is shown in Fig. 9 for a 0.5 mol% Eu-doped LLW crystal fiber. It corresponds to the luminescence decay curve of the $^5D_0 \rightarrow {}^7F_2$ emission. The emission lifetime of 544 μs was obtained fitting experimental data by a single exponential function $I = I_0 \exp(-t/\tau)$ where τ is the $1/e$ lifetime of the Europium ion and I_0 the initial intensity at $t = 0$. The value indicates that no energy transfer is presented in the system and it is similar to other tungstate hosts (Table 3).

4. Conclusions

For the first time, transparent and uniform in diameter, single crystal fibers of Eu^{3+}:LLW and LEW were grown by the μ-PD method in a resistive heating mode and structural and optical characterizations were performed. It was discussed that the pulling rate of growth varies according to the difference between the ionic radii of the alkali and rare earth ions present in the crystal. Despite the fact that in the range of the europium concentration studied only the tetragonal phase was observed in the LLW, Eu:LLW and LEW crystal fibers, Eu^{3+} incorporation induces slightly local distortions in the LLW lattice. Eu^{3+}:LLW single crystal fibers present strong red emission under 395 nm excitation with an observed concentration quenching of around 20 mol% of doping. Excitation spectroscopy was applied to investigate substitution sites for Eu^{3+}. The narrow excitation and emission lines due to the $4f^n \rightarrow 4f^n$ transitions of Eu^{3+} in LLW offer an appropriate method for monitoring the different sites. The symmetry S_4 of the point site is occupied by Eu^{3+} when it partially or totally (LEW case) replaces La^{3+} in the LLW fiber crystals. Regarding the strong emission intensity of Eu:LLW crystal fibers this material reveals itself as a promising matrix for developing near-UV convertible luminescent devices in the red range.

Acknowledgements

The authors acknowledge the Fundação de Amparo à Pesquisa do Estado de São Paulo (FAPESP) (process numbers 96/09604-9, 2006/58686-1, 2008/10721-9) and Conselho Nacional de Pesquisa e Desenvolvimento Científico e Tecnológico (CNPq) (process number 573916/2008-0 – National Institute of Science and Technology in Photonics) for their financial support.

References

[1] X. Huang, Z. Lin, Z. Hu, L. Zhang, J. Huang, G. Wang, J. Cryst. Growth 269 (2004) 401–407.
[2] X. Huang, Q. Fang, Q. Yu, Z. Lü, L. Zhang, Z. Lin, G. Wang, J. Alloys Compd. 468 (2008) 321–326.
[3] X. Huang, Z. Lin, Z. Hu, L. Zhang, T. Tsuboi, G. Wang, Opt. Mater. 29 (2006) 403–406.
[4] X.Y. Huang, Chin. Opt. Lett. 8 (8) (2010) 780–783.
[5] X.Y. Huang, Z.B. Lin, L.Z. Zhang, G.F. Wang, Mater. Res. Innovat. 12 (2) (2008) 94–97.
[6] A.A. Evdokimov, V.K. Trunov, V.I. Spitsyn, Dokl. Akad. Nauk SSSR 207 (1972) 1409–1412.
[7] V.K. Trunov, A.A. Evdokimov, Sov. Phys. Crystallogr. 19 (5) (1975) 616–617.
[8] A.A. Maier, M.V. Provotorov, V.A. Balashov, Russ. Chem. Rev. 42 (10) (1973) 822–833.
[9] G. Huber, W. Lenth, J. Lieberts, F. Lutz, J. Lumin. 16 (1978) 353–360.
[10] E.V. Zharikov, C. Zaldo, F. Díaz, MRS Bull. 34 (2009) 271–276.
[11] Z. Wang, H. Liang, L. Zhou, H. Wu, M. Gong, Q. Su, Chem. Phys. Lett. 412 (2005) 313–316.
[12] L. Yi, X. He, L. Zhou, F. Gong, R. Wang, J. Sun, J. Lumin. 130 (2010) 1113–1117.
[13] C.H. Chiu, M.F. Wang, C.S. Lee, T.M. Chen, J. Solid State Chem. 180 (2007) 619–627.
[14] T. Fukuda, P. Rudolph, S. Uda (Eds.), Fiber Crystal Growth from the Melt, Springer-Verlag, Berlin, 2004.
[15] T. Fukuda, V.I. Chani (Eds.), Shaped Crystals: Growth by Micro-Pulling-Down Technique, Springer-Verlag, Berlin, 2007.
[16] Y. Terada, K. Shimamura, T. Fukuda, J. Alloys Compd. 275–277 (1998) 697–701.
[17] J.R. de Moraes, S.L. Baldochi, S. Ganschow, A.M.E. Santo, A.A. Martin, J. Phys.: Conf. Ser. 249 (2010) 012043.
[18] S.L. Baldochi, F.R. Silva, J.R. de Moraes, J. Jakutis, N.U. Wetter, A.M.E. Santo, J. Cryst. Growth 317 (2011) 4–7.
[19] J.R. de Moraes, Masters' Dissertation, IPEN-University of Sao Paulo, Sao Paulo, 2009. http://www.teses.usp.br/teses/disponiveis/85/85134/tde-11042011-162400/en.php (accessed August 2011).
[20] J.M. Postema, W.T. Fu, D.J.W. Ijdo, J. Solid State Chem. 184 (2011) 2004–2008.
[21] A.C. Larson, R.B. von Dreele, General Structure Analysis System (GSAS), Los Alamos National Laboratory Report LAUR 86-748 (1994).
[22] B.A. Kolesov, L.P. Kozeeva, J. Struct. Chem. 34 (4) (1994) 534–539.
[23] R.D. Shannon, C.T. Prewitt, Acta Crystallogr. A 32 (1976) 751–767.
[24] K.A. Jackson, in: J.J. Metois, P. Rudolph, G. Müller (Eds.), Crystal Growth – From Fundamentals to Technology, Elsevier, Amsterdam, 2004, pp. 27–53.
[25] G.H. Gilmer, in: D.T.J. Hurle (Ed.), Handbook of Crystal Growth 1 – Fundamentals – Part A: Thermodynamics and Kinetics, Elsevier, Amsterdam, 1993, pp. 585–637.
[26] P.V. Klevtsov, L.P. Kozeeva, Sov. Phys. Crystallogr. 15 (1) (1970) 44–47.
[27] P.V. Klevtsov, R.F. Klevtsova, J. Struct. Chem. 18 (1977) 339–355.
[28] K.S. Hwang, S. Hwangbo, J.T. Kim, Ceram. Intern. 35 (2009) 2517–2519.
[29] L.G. van Uitert, in: P. Goldenberg (Ed.), Luminescence of Inorganic Solids, Academic Press, New York, 1966, pp. 465–539.
[30] J.P.M. van Vliet, G. Blasse, L.H. Brixner, J. Solid State Chem. 76 (1988) 160–166.
[31] C.A. Kodaira, H.F. Brito, M.C.F.C. Felinto, J. Solid State Chem. 171 (2003) 401–407.
[32] S. Cotton (Ed.), Lanthanide and Actinide Chemistry, John Wiley & Sons, West Sussex, 2006, pp. 61–83.
[33] O. Chukova, S. Nedilko, V. Scherbatskyi, J. Lumin. 130 (2010) 1805–1812.
[34] Y. Hang, K.H. Jang, K. Jang, H.J. Seo, Physica B 403 (2008) 75–80.
[35] J. Gu, Y. Zhu, H. Li, S. Xiong, X. Zhang, X. Wang, X. Liu, Y. Qian, Solid State Sci. 12 (2010) 1192–1198.